Journal of Catalysis 342 (2016) 67–74

Contents lists available at ScienceDirect

Journal of Catalysis

journal homepage: www.elsevier.com/locate/jcat

Synthesis of Pt nanoparticles with preferential (100) orientation directly on the carbon support for Direct Ethanol Fuel Cell

R.M. Antoniassi, L. Otubo, J.M. Vaz, A. Oliveira Neto, E.V. Spinacé *

Instituto de Pesquisas Energéticas e Nucleares – IPEN-CNEN/SP, Av. Prof. Lineu Prestes, 2242, Cidade Universitária, 05508-900 São Paulo, SP, Brazil

ARTICLE INFO

Article history:
Received 4 May 2016
Revised 28 June 2016
Accepted 26 July 2016
Available online 9 August 2016

Keywords:
Pt nanoparticles
KBr
Electrocatalysts
Fuel cell
DEFC

ABSTRACT

The synthesis of Pt nanoparticles with preferential (100) orientation directly supported on carbon was done by an alcohol-reduction process using KBr as a shape directing agent. The synthesis conditions were varied and the obtained materials were characterized by transmission electron microscopy and cyclic voltammetry. The order of addition of the Pt precursor and KBr was crucial to obtain cubic Pt nanoparticles with small particle size highly dispersed on the carbon support. DEFC experiments showed that Pt nanoparticles with preferential (100) orientation supported on carbon provided superior power densities and CO_2 selectivity compared to supported polycrystalline Pt nanoparticles.

1. Introduction

Coal, oil and natural gas are non-renewable sources that supply the majority of the energy used worldwide. The intensive use of these matrices became a matter of concern especially from an environmental point of view due to emission of greenhouse gases. Thus, much is expected of those technologies that could decentralize the current energy matrix to a clean generation from renewable sources and the use of more efficient energy conversion devices like fuel cells. Among various types of fuel cells, Proton Exchange Membrane Fuel Cell (PEMFC) has received particular attention for potential implementation in portable, mobile and stationary applications. Hydrogen is the fuel used in PEMFC and it is mainly obtained by water electrolysis and steam reforming of hydrocarbons. Electrolysis is a high cost process, consumes a lot of energy and produces hydrogen of high purity, while steam reforming is a cheaper approach, however, the produced hydrogen must be further purified to fuel the PEMFCs. Furthermore, the hydrogen storage still presents a number of difficulties [1]. Instead, the adoption of directly alcohols such ethanol as combustible in fuel cells has attracted great interest, since it is a renewable combustible easily originated from biomass. Direct Ethanol Fuel Cell (DEFC) presents some technological challenges, particularly regarding the anodic catalysis. Due to the difficulty of C—C bond breaking of ethanol molecule, Pt/C electrocatalyst produces principally acetaldehyde and acetic acid and only minor amounts of CO_2, leading to a lower system efficiency. Also, the formation of CO and CH_x intermediates strongly poisons the Pt sites reducing its catalytic activity with time [2–5]. Considering such DEFC challenges, a development of new more efficient electrocatalysts for complete oxidation of ethanol to CO_2 is a promising field to be explored.

Studies have been shown that ethanol electro-oxidation on (100) preferentially oriented Pt nanoparticles is more selective for CO_2 formation when compared to (110) and (111) surfaces [6]. Thus, exposing certain crystallographic facets on the catalyst surface (consequently modifying its morphology) may improve the catalytic activity so as reactional products selectivity. Growth and morphology of the nanoparticles are governed by energy aspects, always following the concept of minimizing the surface energy. All noble metals crystallize in face-centered cubic structure (CFC) and by following the Wulff's construction to predict the shape of nanoparticles [7], surface energy increases according to the direction $\gamma\{111\} < \gamma\{110\} < \gamma\{100\}$, resulting in crystallization in the form of truncated octahedra [8,9]. Eventually, the crystallization process can be modified by the addition of species that interact selectively with the metal surface. Various methods to produce Pt nanoparticles with desired morphological characteristics have been reported in the literature [10–12]. Among them, chemical methods are most suitable, by virtue of providing greater control over the size and shape of the nanoparticles. El-Sayed et al. [13] were the first group to synthesize Pt colloids with different morphologies employing a polymer (sodium polyacrylate) as stabilizing agents. Pt nanoparticles in the form of cubes and tetrahe-

* Corresponding author. Fax: +55 11 3133 9193.
E-mail addresses: espinace@ipen.br, espinace@yahoo.com.br (E.V. Spinacé).

http://dx.doi.org/10.1016/j.jcat.2016.07.022
0021-9517/

drons were produced by modifying the metal/stabilizing agent ratio. Since then, the use of stabilizing agents like polyvinylpyrrolidone (PVP), sodium polyacrilate, oleylamine, has become quite common in colloid synthesis with different morphologies [14,15]. On the other hand, these organic agents might be completely removed from the surface of the nanoparticles before they are used as electrocatalysts in fuel cells, since the surface of Pt nanoparticles is largely blocked by such compounds. Currently methods to remove these impurities normally require great quantities of organic solvents [16], strong oxidizing compounds, like H_2O_2/H_2SO_4 solution [17], or the use of electrochemical oxidation or ultraviolet irradiation techniques [18,19]. Besides, aggregation and destruction of nanoparticles are still reported [20] making this approach impractical for large applications. It also could be considered that Pt nanoparticles must be further anchored on carbon to be used as electrocatalyst in PEMFC. Thus, the preparation of Pt nanoparticles with desired morphology and free of organic surface impurities is a major challenge. Solla-Gullón and collaborators [21,22] prepared cubic Pt nanoparticles with a preferential (100) surface structure by a water-in-oil microemulsion method using HCl or H_2SO_4 as surface modifiers in the water phase. The obtained Pt nanoparticles showed good performance for ammonia and CO electro-oxidations, which are (100) structure-sensitive reactions. Recently, these Pt nanoparticles were supported on a carbon with different metal loadings and tested for ammonia and acid formic electro-oxidation [23]. Kim et al. [24] prepared Pt cubes directly nucleated and overgrown on support by reducing Pt precursors in the presence of carbon supports and anchoring agents, like cysteamine. The obtained materials showed superior activity and long-term stability for oxygen reduction reaction. Cheng et al. [25] prepared Pt nanocubes on various supports by reducing Pt precursor under a CO atmosphere in benzyl alcohol and their materials exhibited high activity for methanol electro-oxidation.

The synthesis of Pt nanoparticles with (100) preferential orientation directly supported on carbon and their application as anodic catalysts in DEFC is extremely rare in the literature. Recently, Figueiredo et al. [26] supported (100) preferentially oriented Pt nanoparticles, prepared by a water in oil microemulsion method as described in reference [21] and used as anodes for DEFC. They have showed the benefit of these faceted materials in fuel cell performance when compared with cuboctahedral Pt nanoparticles and polycrystalline commercial Pt catalyst.

Halide ions and other small anions [27] has a strong tendency to adsorb on the metal surface and results in a surface energy modification, leading to an anisotropic growth; however, such ions could be removed by a feasible water washing process. In this work, we describe a simple synthesis strategy to prepare Pt nanoparticles with preferential (100) orientation directly supported on carbon using only bromide ions as shape directing agent.

2. Experimental

2.1. Preparation of Pt nanoparticles with preferential (100) orientation directly on the carbon support (Pt/C electrocatalysts)

The following materials were used: hydrated hexacloroplatinum(IV) acid ($H_2PtCl_6{\cdot}6H_2O$, 99.95% purity) as metal source, potassium bromide (KBr, 99.7%), Vulcan Carbon (X72R – Cabot Corporation), deionized water and ethylene glycol (EG). Pt/C (20 wt% of metal load) electrocatalysts were prepared by an alcohol-reduction process [28] by adding $H_2PtCl_6.6H_2O$ and KBr into a EG:H_2O 3:1 (v:v) solution. The carbon support was added into this solution, which was submitted for 5 min in an ultrasonic bath. The resulting mixture was kept under reflux at 150 °C for 3 h before being filtered, washed with abundant water and dried for 2 h at 80 °C. Others parameters evaluated were the order of addition of $H_2PtCl_6{\cdot}6H_2O$ and KBr and the amounts (wt%) of $H_2PtCl_6{\cdot}6H_2O$ added at different steps.

2.2. Physico-chemical characterizations

Size, dispersion and morphology of Pt nanoparticles were evaluated by transmission electron microscopy (TEM –JEOL model JEM 2100, operating at 200 kV). For TEM analysis, an amount of the electrocatalyst was suspended in isopropyl alcohol and dropped in TEM cupper-grid coated with collodion film. The size was measured by end-to-end particle's extension. X-ray diffraction analyses were performed using a Rigaku diffractometer model Miniflex II, using Cu Kα radiation source (λ = 0.15406 nm). The diffractograms were recorded in the range of 2θ between 20° and 90° with a step size of 0.05° and a scan time of 2 s per step.

Cyclic voltammetry technique (CV) was employed for electrochemical and surface studies, using a 910 PSTAT (Metrohm) potentiostat. A three-electrodes cell system with an ultrathin vitreous carbon layer previously polished was used as work electrode, a platinum plate as counter electrode and hydrogen electrode (HRE) as reference. An aliquot of 10 μL of ultrasonicated catalytic ink containing water (0.9 mL), isopropyl alcohol (0.1 mL), Nafion solution 5% (0.02 mL) and the catalytic powder (1 mg) was dropped on the tip of vitreous carbon and let air dried. Sulfuric acid medium (0.5 mol L^{-1}) was used as electrolyte. After nitrogen gas was bubbled into H_2SO_4 solution for 30 min, CVs were recorded at 50 mV s^{-1} at ambient temperature.

2.3. Single DEFC electrical performance

For MEAs (Membrane Electrode Assembly) preparation, synthesized Pt/C electrocatalysts were tested as anodes (1 mg Pt cm^{-2}) while commercial Pt/C (purchased from BASF, lot# F0381022) was chosen as cathode (1 mg Pt cm^{-2}). Both 5 cm^2 electrodes were hot pressed to a pretreated Nafion 115 membrane (Dupont) electrolyte at 125 °C for 10 min. All prepared MEAs were inserted in a single cell, operating at 100 °C, fueled with 2 mL min^{-1} of ethanol (2 mol L^{-1}) and 500 mL min^{-1} of oxygen at 2 bar. Polarization and power density curves were employed to determine the real DEFC electrical performance of the synthesized catalysts.

2.4. Products distribution by gas chromatography

The products of ethanol electro-oxidation were determined and quantified by gas chromatography using a gas chromatograph (GC), model Agilent 7890 A. For these experiments a capillary column Plot-U (30 m) and a thermal conductivity detector (TCD) were employed. The elution gas was carried out using hydrogen gas with a flow rate of 45 mL min^{-1} and the oven temperature was maintained at 80 °C for 5 min and, afterward, it was increased at 10 °C min^{-1} until reach 160 °C. Inlet and detector temperatures were set to 180 °C and 220 °C, respectively. An aliquot (collected at maximum power density condition) of anodic effluent of the single cell was cooled in an ice bath before to be manually injected into GC.

The selectivity (S) was based on total amount of the reaction products from the anodic effluent and it was calculated by Eq. (1):

$$\%S_i = \left(\frac{C_i}{C_{AAL} + C_{AA} + C_{CO_2}}\right)100\% \quad (1)$$

where C is the concentration of the product i; acetaldehyde (AAL), acetic acid (AA) and CO_2. The products were quantified using calibration curves.

3. Results and discussion

Initially, we observed how the morphological characteristics of Pt nanoparticles were affected by the presence of different KBr quantities. Pt/C syntheses were performed by adding the total amount of $H_2PtCl_6.6H_2O$, KBr and carbon into EG/H_2O solution. Fig. 1 shows TEM micrographs of prepared Pt/C electrocatalysts with Br^-:Pt ratios varying from 0 to 500. It can be clearly seen that both size and morphology of Pt nanoparticles (PtNPs) were changed as result of KBr increasing. TEM images show spherical shaped PtNPs with an average size of approximately 4 nm for both Pt/C prepared in the absence of KBr and Pt/C with Br^-:Pt ratio of 10 (Fig. 1a and b). Curiously, when this ratio increases to 60 (Fig. 1c) two particle size domains were observed, one of 4 nm nanoparticles with spherical shape, as observed previously, and another containing agglomerated PtNPs with an undefined morphology and sizes about 26 nm. Increasing the Br^-:Pt ratio to 150 (Fig. 1d) small nanoparticles with spherical shape are no longer observed but agglomerated particles with mean size around 44 nm were found. For 300 (subsequently called Pt/C 100) and 500 Br^-:Pt ratio (Fig. 1e and f), PtNPs assumed a cubic shape tendency. Besides of being poorly dispersed on some concentrated regions of the carbon surface, the particle sizes were one order of magnitude higher than Pt/C. It must be highlighted that in catalytic terms nanoparticles are size-dependent, since smaller ones expose a higher surface area per volume, increasing the number of active sites and thus benefiting the catalytic activity. Cubic particles are interesting to DEFC anodes; however these cubic PtNPs shown in Fig. 1 were far from the ideal conditions for a catalytic application, being necessary a better control over the size, shape and distribution on the support. Consequently, a systematic study of the syntheses parameters were carried out in order to obtain small cubic nanoparticles dispersed on carbon surface. A scheme is shown in Fig. 2 (route A, B and C). Initially, the synthesis was performed in a single step, in which the total amount of H_2PtCl_6 and KBr were added at the beginning of the synthesis (route A). As a new strategy to obtain small sized PtNPs in cubical shape, the KBr amount needed to achieve cubic PtNPs (Br^-:Pt 300) was maintained, but part of the H_2PtCl_6 and the total amount of KBr were added at the beginning of the synthesis and, after a determined time of reaction, the remainder of H_2PtCl_6 was added (route B). In this manner, part of the platinum source was initially used to form nuclei (or seeds) of Pt^0 on the carbon support. TEM micrographs of the obtained materials were shown in Fig. 3 and it is clearly seen a drastic change in particle sizes and distribution after applying the strategy mentioned. Fig. 3a showed the material prepared in a single step, which 100 wt% of platinum precursor and KBr were added at the beginning of the reaction. In this case, the reduction of Pt(IV) ions occurred in the presence of KBr, leading to the formation of cubic aggregates of ~55 nm (see also Fig. 1e) that were formed of smaller 5–9 nm cubic subunits (yellow highlighted from inset). Fig. 3b showed the material prepared in two steps (Pt/C 10.90), in which 10 wt% of the amount of Pt precursor was added at the beginning of the synthesis with 100 wt% of KBr. The reaction was allowed to proceed for 30 min at 150 °C and, after this period, the 90 wt% Pt precursor remainder was added. The material showed an improved dispersion of PtNPs on the carbon support and the presence of cubic nanoparticles were around 5 nm, however, aggregated particles formed of small cubic subnits were still verified. Thus, two particle size domains were observed in this material as pointed by red arrows in Fig. 3b. Following the same procedure, it is worthy to say that different amounts of Pt precursor were added at the beginning of the synthesis (from 10 wt% to 90 wt% - TEM micrographs not shown here), however the smaller particle size domain was suppressed as the dedicated initial percentage was increased while the PtNPs sizes enlarged. Another strategy (route C) was to add only part of the amount of H_2PtCl_6 at the beginning of the synthesis process and after a determined time of reaction, the total amount of KBr was injected. Then, the reaction proceeds for a further period until the remainder amount of H_2PtCl_6 was quickly added. In this case, 30 wt% of Pt precursor was added in the beginning of the synthesis and the reaction was allowed to proceed for 15 min at 150 °C. This time was sufficient to occurs the reduction of Pt(IV) ions leading to the formation of Pt seeds (nucleation stage). Then, 100 wt% of KBr was added and after 20 min, the remaining amount Pt precursor was quickly injected. Fig. 3c showed the micrograph of the obtained material (called by Pt/C 30.70) and it is remarkable that the major part of Pt nanoparticles exhibited a cubic morphology and particle sizes in the range of 6–8 nm dispersed on carbon; interestingly, the formation of bigger particles or aggregates were not observed. The high resolution image in Fig. 3d exhibits in detail a cubic Pt nanoparticle where it is possible to observe the atomic lattice fringes. The interplanar measured distance of 1.99 Å represents the $d_{(200)}$ enclosed facets, which are extended until the cube exposed faces, thus confirming the formation of Pt nanoparticles with preferential (100) orientation. X-ray diffraction of Pt/C 30.70 (Fig. 4) showed a peak at about $2\theta = 25°$ due to the carbon support and five peaks at about $2\theta = 40°$, 46°, 68°, 81° and 85° corresponding to (111), (200), (220), (311) and (221) crystallographic planes of face-centered cubic (fcc) phase of Pt [28]. Comparing the intensities ratio between (200) and (111) diffraction peaks, Pt/C prepared in the absence of KBr exhibited a ratio of 38% while for Pt/C 30.70 the ratio increased to 46%. This result also indicates the formation of Pt nanoparticles with preferential (100) orientation for Pt/C 30.70 electrocatalyst [29].

According to our results, it could be observed the formation of cubes happens only under higher bromide quantities in relation to Pt. On the other hand, it was checked the PtNPs agglomeration also occurs with the increase of Br^-:Pt ratio. Based on these results an intriguing question arises: Could a particle, already supported, evolve to cubic shape by just adding bromide? A new type of experiment was performed, in which 100 wt% of Pt precursor was reduced on carbon support during a determined period before the KBr (Br^-:Pt ratio of 300) addition. The morphology was monitored during different times by ceasing the syntheses. Fig. 5a

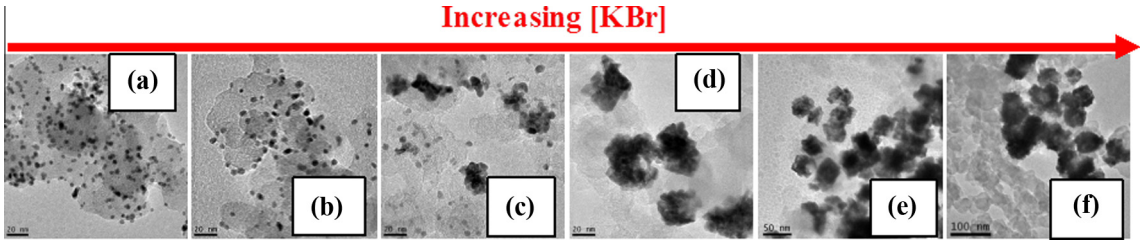

Fig. 1. TEM micrographs of Pt/C electrocatalysts (a) without KBr (4,2 ± 1 nm), (b) Br^-:Pt ratio of 10 (4,3 ± 1 nm), (c) Br^-:Pt ratio of 60 (4,2 ± 0,9 e 26,4 ± 7,9 nm), (d) Br^-:Pt ratio of 150 (43,9 ± 11,2 nm), (e) Br^-:Pt ratio of 300 (46,4 ± 8,2 nm) and (f) Br^-:Pt ratio of 500 (54,2 ± 9,9 nm).

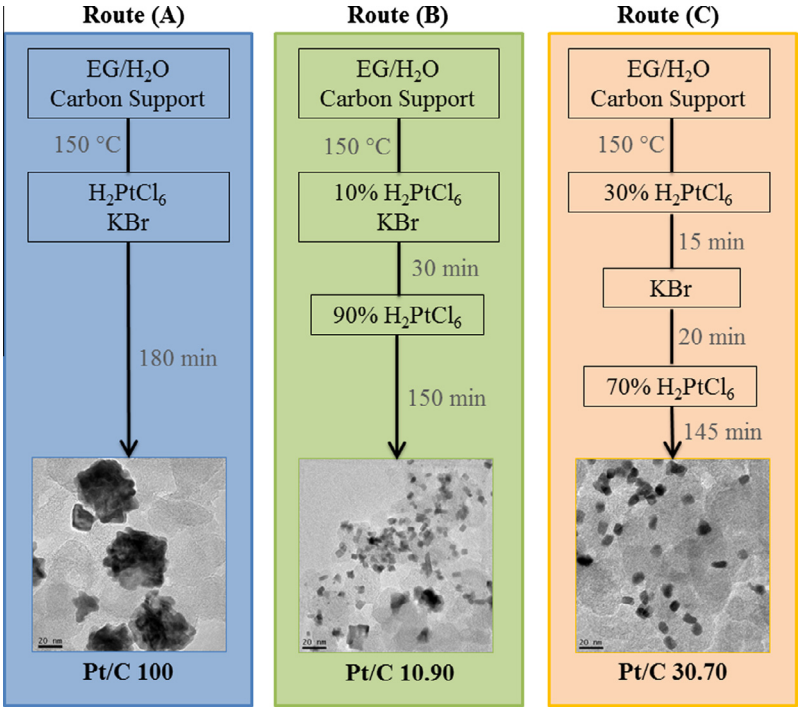

Fig. 2. Different routes used to prepare Pt/C electrocatalysts.

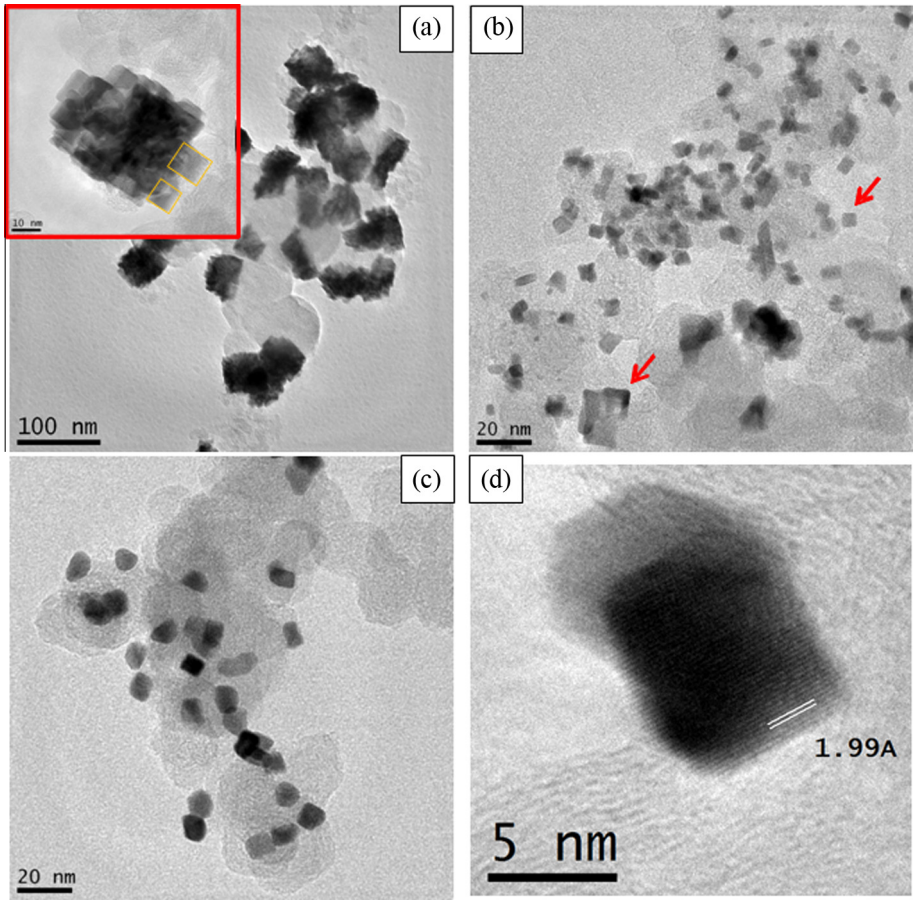

Fig. 3. TEM micrographs of Pt/C electrocatalysts prepared with Br^-:Pt ratio of 300 under different conditions (a) addition of Pt source and KBr at the beginning of the synthesis (single step), (b) addition of part of Pt source with KBr at the beginning of the synthesis and the remainder of Pt source after a determined period, (c) addition of part of Pt source at the beginning of the synthesis, after a determined period addition of KBr and after that addition of the remainder Pt source and (d) detail of a cube from (c).

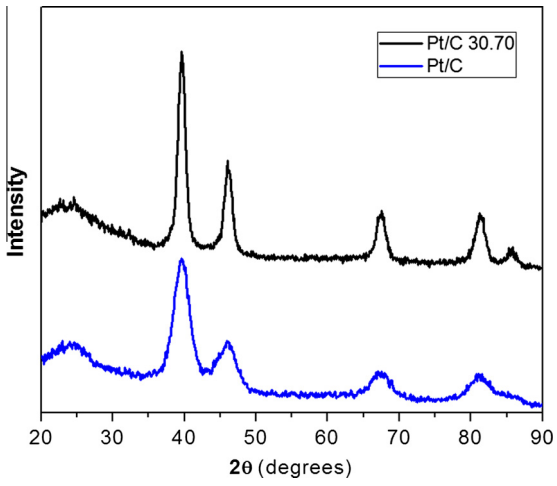

Fig. 4. X-ray diffractograms of Pt/C 30.70 electrocatalyst and Pt/C prepared in the absence of KBr.

showed the material obtained after 15 min from KBr addition. The material prepared in absence of KBr (Fig. 1a) exhibited spherical shape and highly dispersed PtNPs on carbon. After KBr addition there were no cubic particles but an agglomeration of spherical PtNPs were observed. After 30 min (Fig. 5b) and 3 h (Fig. 5c) from KBr addition, only an increase of the agglomeration continues to occur. Thus, we could conclude that after Pt nanoparticles were formed, Br^- ions lead only to their agglomeration. Thus, to obtain cubic Pt nanoparticles, Pt ions and bromide ions must coexist in the reaction medium.

Different amounts of Pt precursor added before and after the addition of KBr were also studied to control the portion of initial seeds (route C). Cubes with 7 nm and highly dispersed on carbon support were observed when 30 wt% of H_2PtCl_6 was destined for seed formation (Fig. 6a), while a poor cubic selectivity and some agglomerated particles were observed (Fig. 6b) when 70 wt% of H_2PtCl_6 was used (named Pt/C 70.30). When the initial portion of precursor was increased to 90 wt% (Pt/C 90.10), no more cubes were observed (Fig. 6c). Thus, based on all these evaluation of synthesis parameters, we could infer some aspects of PtNPs formation: when the quantity of Pt precursor in the first step is high, the formation of Pt nanoparticles occurs and, in the presence of KBr, they are preferentially agglomerated. Also, in this case, there is a small amount of Pt precursor to be reduced over the surface of the already formed Pt nanoparticles. On the other hand, when the quantity of the Pt precursor in the first step is low, the formation of small Pt nanoparticles (seeds) occurs and, in the presence of KBr, the reduction of the remainder amount Pt(IV) ions over the Pt seeds surface leads to the formation of cubic Pt nanoparticles with preferential (100) orientation and with good dispersion on the carbon support. It is clearly observed that an agglomeration phenomenon becomes notable as the amounts of Pt precursor used to nucleate seeds increases. This again confirms the KBr influence in grouping the particles.

In order to investigate the morphology development of Pt/C 30.70 electrocatalyst, some aliquots of the material were collected at different synthesis times and analyzed by TEM (Fig. 7). After 10 min of 30 wt% of H_2PtCl_6 addition, TEM micrograph showed Pt nanoparticles with spherical shape dispersed on the carbon support with an average size of 4 nm, as already observed for Pt/C prepared in the absence of KBr (Fig. 1a). A slightly increase in nanoparticle size (from 4 to 5.5 nm) is verified after 10 min of KBr addition; however, Pt nanoparticles with spherical shapes continue to be observed. This increase of size could be due nanoparticles agglomeration as already observed in Fig. 5a. Pt nanoparticles with cubic shape were only observed after adding the remainder H_2PtCl_6 showing that the reduction of the remainder Pt(IV) ions must occurs in the presence of Pt seeds and KBr to achieve the desired size and morphology. Thus, it is possible to observe some cubes with average size in the range of 4–6 nm after 10 min of the addition of the remainder H_2PtCl_6. Finally, after 3 h of synthesis it could be seen that cubic PtNPs with average size in the range of 6–8 nm were preferentially formed.

Cyclic voltammograms (CV) were recorded to verify the basal Miller planes of the different Pt/C catalysts prepared with Br^-:Pt ratio of 300. CVs were collected in 0.05–0.8 V range cycles in order to avoid the structure destruction, since cycles beyond 1 V may result in a reassemble of surface atoms, hence the loss of crystal characteristics of the material [30]. Arán-Ais et al. [31] studied changes in the shape and morphology of shaped Pt nanoparticles as a result of electrochemical cycling and found a rapidly degradation of Pt nanoparticles as a result of potencial cycling up to +1.3 V. Based on investigations of hydrogen dessorption (cathodic scan) on Pt monocrystals [32] and shaped-controlled Pt nanoparticles [33], the peak close to 0.125 V corresponds to the process in (110)-type sites, the peak at 0.27 V contain two contributions from (100) step sites on (111) terraces and the signals at 0.35–0.37 V attributed to (100) bidimensional terraces. In Fig. 8a are shown the CVs recorded into 0.5 mol L^{-1} of H_2SO_4 at 50 mV s^{-1} and they are in accordance to expected Pt profile in acid media [33]. From the figure inset, it is possible to verify for Pt/C prepared without KBr addition that the contribution (100) is less intense than that one for (110) peak and no signals where observed at 0.35–0.37 V. For Pt/C 90.10 electrocatalyst, where no cubic nanoparticles are seen in micrographs (Fig. 6c), a similar CV profile was observed. However, for Pt/C 30.70 (Fig. 6a) and Pt/C 70.30 (Fig. 6b), where cubic nanoparticles are seen in the micrographs, the contribution (100) became greater than (110) and the contribution at around

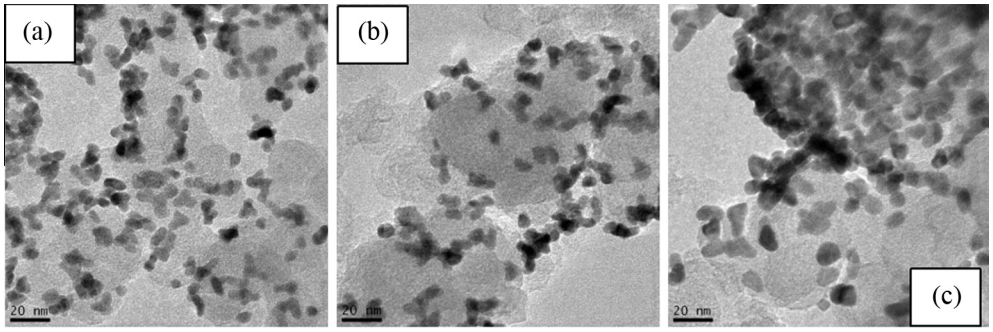

Fig. 5. TEM micrographs of Pt/C electrocatalyst prepared with Br^-:Pt ratio of 300 being KBr added only after completely Pt reduction (a) after 15 min of KBr addition, (b) after 30 min and (c) after 3 h.

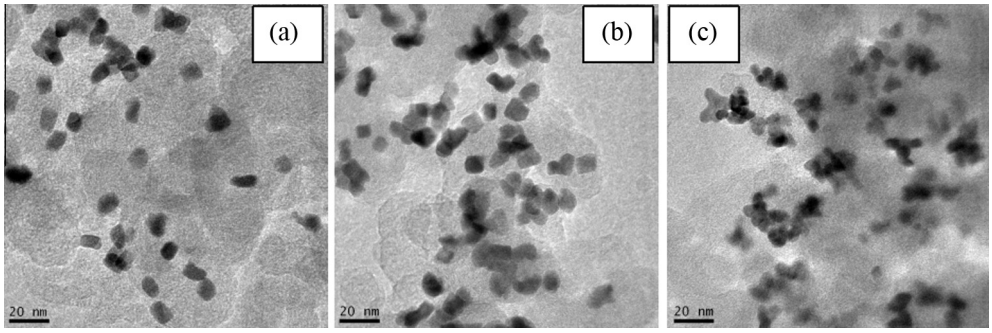

Fig. 6. TEM micrographs of Pt/C electrocatalysts prepared with Br^-:Pt ratio of 300 using route C (a) addition of 30 wt% of Pt source at the beginning of the synthesis (15 min under reflux) followed by KBr addition and after 20 min the remainder 70 wt% of Pt source (b) same procedure before, but modifying the initial and final amounts of Pt source to 70 wt% and 30 wt%, respectively, and (c) the initial and final amounts of Pt source of 90 wt% and 10 wt%.

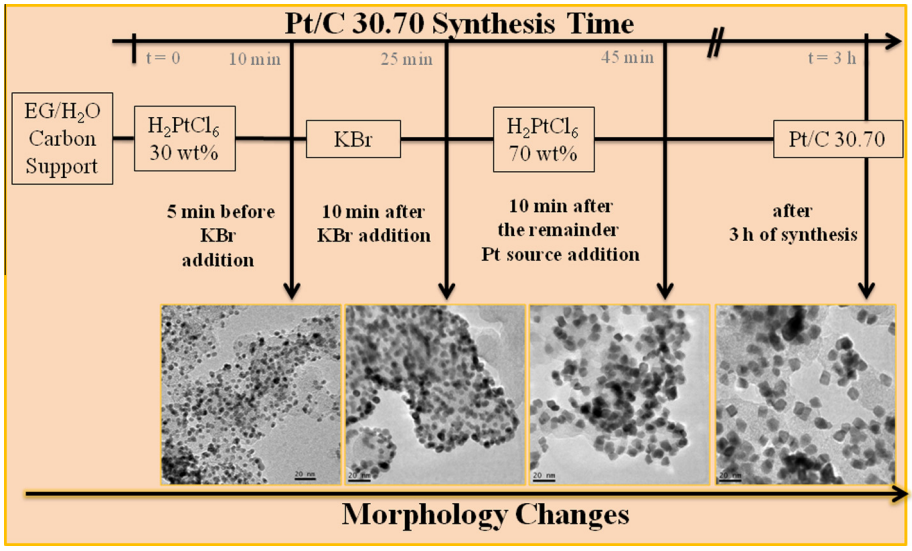

Fig. 7. Morphology development of Pt/C 30.70 electrocatalyst (collected at different synthesis times and analyzed by TEM).

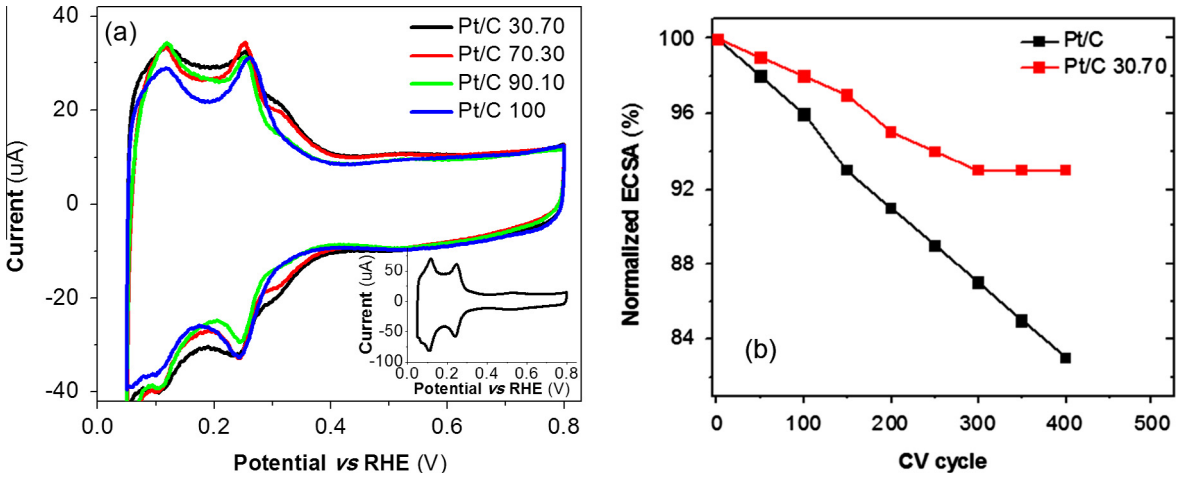

Fig. 8. CVs of Pt/C electrocatalysts prepared with Br^-:Pt ratio of 300 under different conditions: (a) H_2SO_4 0.5 mol L^{-1} electrolyte and scan rate of 50 mV s^{-1} and (b) ECSA loss with CV cycling.

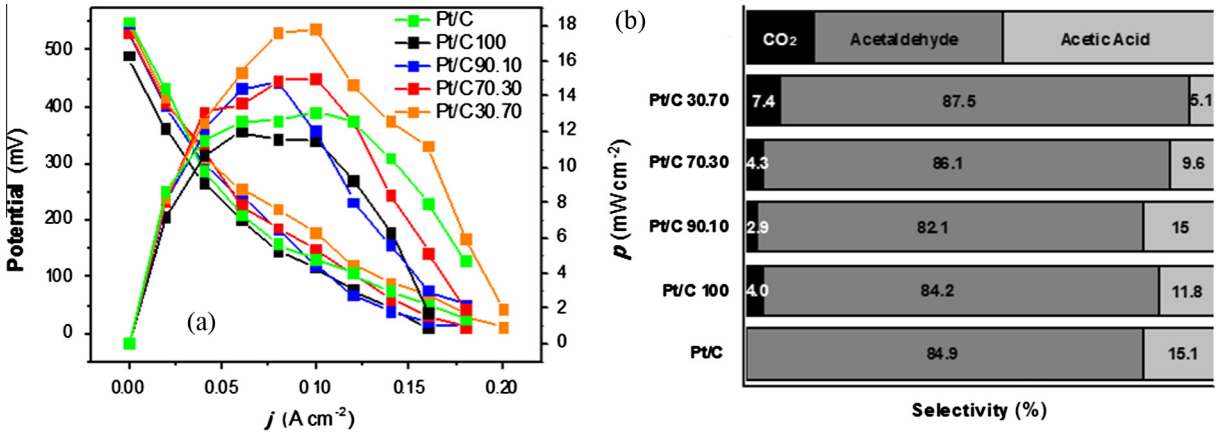

Fig. 9. (a) Polarization and power density curves for the prepared Pt/C electrocatalyts used as anodes and commercial Pt/C as cathode and (b) products selectivity of ethanol electro-oxidation evaluated by gas chromatography.

0.35 V was evident for these samples confirming the cubes exposed facets. On the other hand, the contribution at 0.35 V is considerably less defined than that observed with unsupported cubic Pt nanoparticles [33]. Probably, this could be due to less uniformity of the obtained supported Pt nanoparticles compared to the unsupported ones [33] and/or to the fact that the carbon support can affect the definition of this contribution.

Stability of Pt/C 30.70 and Pt/C electrocatalysts was verified by ECSA loss over 400 CV cycles (Fig. 8b). A quick and continuous drop in ECSA values was observed for Pt/C while Pt/C 30.70 reached equilibrium over the 300th, losing only 7% from its normalized data. This indicates a good resistance of cubic Pt/C 30.70 structure even under high applied potentials conditions. Besides, Pt(100) facets were preserved during all the 400 cycles, indicating the morphology was maintained.

DEFC experiments were carried out with MEAs containing as anodic electrocatalysts Pt/C prepared without the addition of KBr and the materials prepared in the presence of KBr in different conditions: Pt/C 100, Pt/C 90.10, Pt/C 70.30, Pt/C 30.70 and Pt/C (prepared in the absence KBr). Commercial Pt/C from BASF was maintained in cathode. The electric performances are exhibited in Fig. 9a. Pt/C 100 synthesized by a single step showed the lower electrical performance, for both open circuit potential (OCP) and maximum power density, 489 mV and 12 mW cm^{-2}, followed by Pt/C 90.10 with 532 mV and 14.5 mW cm^{-2}, respectively. The superior power densities were provided by Pt/C 70.30 (15 mW cm^{-2}) and Pt/C 30.70 (18 mW cm^{-2}), value almost 40% greater than Pt/C prepared in the absence of KBr.

The DEFC electrical performance is a result of ethanol electrochemical oxidation, forming CO_2, acetaldehyde and acetic acid products. Aliquots of the anodic effluent were collected at a maximum power density condition (about 0.1 A cm^{-2} for all electrocatalysts) and analyzed by gas chromatography (Fig. 9b). The highest CO_2 production was obtained by Pt/C 30.70 electrocatalyst, evidencing the ability of Pt(100) sites in oxidizing ethanol molecule completely. This value is 72% higher than Pt/C 70.30 and 84% to Pt/C 100. It is worthy to note that in such conditions Pt/C did not produce detectable quantities of CO_2. Recently, Buró-Rogero et al. [34] studied ethanol electro-oxidation on (100) and (111) preferentially oriented Pt nanoparticles using ATR-FTIR and DEMS techniques and observed that in spite of the fact that the incomplete ethanol oxidation was observed for both samples, a high activity for the formation of C-1 fragments (CO_{ads} and $CH_{x\,ads}$) as intermediates was observed for (100) domains. The CO_2 efficiency was higher for (100) than for (111) Pt nanoparticles, where CO_{ads} formation and C—C bond breaking of ethanol molecule were hindered, promoting the formation of acetaldehyde and acetic acid. The authors concluded that these results are in agreement with previous studies done with single crystal electrodes. In a similar way, an increase of CO_2 selectivity was also observed in this work using Pt nanoparticles with (100) preferential orientation supported on carbon as anode in DEFC. The catalytic performance of Pt nanoparticles is influenced by the size, shape and composition; however, surface defects like step and kink atoms with low coordination numbers should also be considered [35–38]. Studies on ethanol electro-oxidation have been shown that high-index faceted Pt nanoparticles with low-coordinate step atoms [35,36] and stepped Pt single crystal electrodes [37] can improve the catalytic activity and selectivity. These results clearly showed the importance of the surface structure of Pt nanoparticles for ethanol electro-oxidation in DEFC. Thus, we are now dedicating efforts to produce an alloyed PtSn in cubical shape and dispersed Pt cubes on SnO_2/C as electrocatalysts for DEFC [39,40].

4. Conclusions

A simple methodology was developed to prepare cubic Pt nanoparticles with preferential (100) orientation directly on the carbon support without the use of organic additives as a shape-directing or capping agents. KBr was used as a shape-directing agent and the Br^-:Pt molar ratio defined the morphology of the obtained Pt nanoparticles. Through variations in the synthesis conditions like the order of addition of the Pt precursor and KBr, as well, the amounts of Pt precursor added at different steps of synthesis process lead to the formation of well-dispersed cubic Pt nanoparticles with preferential (100) orientation directly supported on carbon providing superior power densities and CO_2 selectivity for DEFC when compared to supported polycristalline Pt nanoparticles.

Acknowledgments

The authors thanks CNPq Proc. nº 310051/2012-6 and 443046/2014-0 and FAPESP Proc. nº 2014/09087-4 for financial support.

References

[1] M. Balat, Int. J. Hydrogen Energy 33 (2008) 4013–4029.
[2] G.A. Camara, R.B. de Lima, T. Iwasita, J. Electroanal. Chem. 585 (2005) 128–131.
[3] V. Pacheco Santos, V. Del Colle, R.B. de Lima, G. Tremiliosi-Filho, Electrochim. Acta 52 (2007) 2376–2385.

[4] G. García, N. Tsiouvaras, E. Pastor, M.A. Peña, J.L.G. Fierro, M.V. Martínez-Huerta, Int. J. Hydrogen Energy 37 (2012) 7131–7140.
[5] S. Rousseau, C. Coutanceau, C. Lamy, J.-M. Léger, J. Power Sources 158 (2006) 18–24.
[6] C. Buso-Rogero, V. Grozovski, F.J. Vidal-Iglesias, J. Solla-Gullón, E. Herrero, J.M. Feliu, J. Mater. Chem. A 24 (2013) 7068–7076.
[7] Y. Xia, X. Xia, H.C. Peng, J. Am. Chem. Soc. 137 (2015) 7947–7966.
[8] N. Tian, Z.Y. Zhou, S.G. Sun, J. Phys. Chem. C 112 (2008) 19801–19817.
[9] B. Lim, Y. Xia, Angew. Chem. Int. Ed. 50 (2011) 76–85.
[10] W. Zhang, J. Yang, X. Lu, ACS Nano 6 (2012) 7397–7405.
[11] M. Tsuji, Y. Nishizawa, K. Matsumoto, N. Miyamae, T. Tsuji, X. Zhang, Colloids Surf. A 293 (2007) 185–194.
[12] Y. Ma, Q. Kuang, Z. Jiang, Z. Xie, R. Huang, L. Zheng, Angew. Chem. Int. Ed. 47 (2008) 8901–8904.
[13] T.S. Ahmadi, Z.L. Wang, A. Henglein, M.A. El-Sayed, Chem. Mater. 8 (1996) 1161–1163.
[14] M.H. Huang, C.-A. Chiu, J. Mater. Chem. A 98 (2013) 8081–8092.
[15] N. Naresh, F.G.S. Wasim, B.P. Ladewig, M. Neergat, J. Mater. Chem. A 30 (2013) 8553–8559.
[16] J.M. Krier, W.D. Michalak, L.R. Baker, K. An, K. Komvopoulos, G.A. Somorjai, J. Phys. Chem. C 116 (2012) 17540–17546.
[17] J. Monzó, M.T.M. Koper, P. Rodriguez, ChemPhysChem 13 (2012) 709–715.
[18] P.S. Fernández, D.S. Ferreira, C.A. Martins, H.E. Troiani, G.A. Camara, M.E. Martins, Electrochim. Acta 98 (2013) 25–31.
[19] D. Li, C. Wang, D. Tripkovic, S. Sun, N.M. Markovic, V.R. Stamenkovic, ACS Catal. 2 (2012) 1358–1362.
[20] J.A. Michel, W.H. Morris, C.M. Lukehart, J. Mater. Chem. A 5 (2015) 2012–2018.
[21] R.A. Martínez-Rodríguez, F.J. Vidal-Iglesias, J. Solla-Gullón, C.R. Cabrera, J.M. Feliu, J. Am. Chem. Soc. 136 (2014) 1280–1283.
[22] R.A. Martínez-Rodríguez, F.J. Vidal-Iglesias, J. Solla-Gullón, C.R. Cabrera, J.M. Feliu, ChemPhysChem 15 (2014) 1997–2001.
[23] F.J. Vidal-Iglesias, V. Montiel, J. Solla-Gullón, J. Solid State Electrochem. 20 (2016) 1107–1118.
[24] C. Kim, S.S. Kim, S. Yang, J.W. Han, H. Lee, Chem. Commun. 48 (2012) 6396–6398.
[25] G. Chen, Y. Tan, B. Wu, G. Fu, N. Zheng, Chem. Commun. 48 (2012) 2758–2760.
[26] M.C. Figueiredo, J. Solla-Gullón, F.J. Vidal-Iglesias, M. Nisula, J.M. Feliu, T. Kallio, Electrochem. Commun. 55 (2015) 47–50.
[27] N. Ortiz, S.E. Skrabalak, Langmuir 30 (2014) 6649–6659.
[28] R.M. Antoniassi, A. Oliveira Neto, M. Linardi, E.V. Spinacé, Int. J. Hydrogen Energy 38 (2013) 12069–12077.
[29] X. Zhang, H. Yin, J. Wang, L. Chang, Y. Gao, W. Liu, Z. Tang, Nanoscale 5 (2013) 8392–8397.
[30] R. Devivaraprasad, R. Ramesh, N. Naresh, T. Kar, R.K. Singh, M. Neergat, Langmuir 30 (2014) 8995–9006.
[31] R.M. Arán-Ais, Y. Yu, R. Hovden, J. Solla-Gullón, E. Herrero, J.M. Feliu, H.D. Abruña, J. Am. Chem. Soc. 137 (2015) 14992–14998.
[32] V.P. dos Santos, G. Tremiliosi Filho, Quím. Nova 24 (2001) 856–863.
[33] F.J. Vidal-Iglesias, R.M. Arán-Ais, J. Solla-Gullón, E. Herrero, J.M. Feliu, ACS Catal. 2 (2012) 901–910.
[34] C. Busó-Rogero, S. Brimaud, J. Solla-Gullon, F.J. Vidal-Iglesias, E. Herrero, R.J. Behm, J.M. Feliu, J. Electroanal. Chem. 763 (2016) 116–124.
[35] Z.-Y. Zhou, Z.-Z. Huang, D.-J. Chen, Q. Wang, N. Tian, S.-G. Sun, Angew. Chem. Int. Ed. 49 (2010) 411–414.
[36] L. Zhang, D. Chen, Z. Jiang, J. Zhang, S. Xie, Q. Kuang, Z. Xie, L. Zheng, Nano Res. 5 (2012) 181–189.
[37] F. Colmati, G. Tremiliosi-Filho, E.R. Gonzalez, A. Berná, E. Herrero, J.M. Feliu, Phys. Chem. Chem. Phys. 11 (2009) 9114–9123.
[38] S. Xie, Q. Xu, X. Huang, ChemCatChem 8 (2016) 480–485.
[39] F.L.S. Purgato, S. Pronier, P. Olivi, A.R. de Andrade, J.M. Léger, G. Tremiliosi-Filho, K.B. Kokoh, J. Power Sources 198 (2012) 95–99.
[40] B. Liu, Z.W. Chia, Z.Y. Lee, C.H. Cheng, J.Y. Lee, Z.L. Liu, Fuel Cells 12 (2012) 670–676.